

# Ethanol Dehydration Pathways on NASICON-Type $A_{0.33}M_2(PO_4)_3$ (A=Dy, Y, Yb); M = Ti, Zr) catalysts: The Role of Hydroxyl Group Proton Mobility in Selectivity Control

[Anna I. Zhukova](#)<sup>\*</sup>, Alina D. Sazonova, [Andrey N. Kharlanov](#), [Elena A. Asabina](#), [Vladimir I. Pet'kov](#), [Vladislav A. Sedov](#), Vasiliy D. Prokhin, [Diana A. Osaulenko](#), Yuri A. Fionov, Irina I. Mikhaleiko, Elena A. Fionova, Dmitry Yu. Zhukov

Posted Date: 30 April 2025

doi: 10.20944/preprints202504.2561.v1

Keywords: dehydration; diethyl ether; ethylene; Brønsted sites; titanium phosphate; zirconium phosphate; rare-earth elements



Preprints.org is a free multidisciplinary platform providing preprint service that is dedicated to making early versions of research outputs permanently available and citable. Preprints posted at Preprints.org appear in Web of Science, Crossref, Google Scholar, Scilit, Europe PMC.

Copyright: This open access article is published under a Creative Commons CC BY 4.0 license, which permit the free download, distribution, and reuse, provided that the author and preprint are cited in any reuse.

## Article

# Ethanol Dehydration Pathways on NASICON-Type $A_{0.33}M_2(PO_4)_3$ (A=Dy, Y, Yb); M = Ti, Zr) catalysts: The Role of Hydroxyl Group Proton Mobility in Selectivity Control

Anna I. Zhukova <sup>1,\*</sup>, Alina D. Sazonova <sup>1</sup>, Andrey N. Kharlanov <sup>2</sup>, Elena A. Asabina <sup>3</sup>, Vladimir I. Pet'kov <sup>3</sup>, Vladislav A. Sedov <sup>3</sup>, Vasiliy D. Prokhin <sup>3</sup>, Diana A. Osaulenko <sup>1</sup>, Yuri A. Fionov <sup>1</sup>, Irina I. Mikhaleenko <sup>1</sup>, Elena A. Fionova <sup>2</sup> and Dmitry Yu. Zhukov <sup>4</sup>

<sup>1</sup> Department of Physical and Colloid Chemistry, Peoples Friendship University of Russia (RUDN University), 6, Miklukho-Maklaya Str., Moscow 117198

<sup>2</sup> Department of Chemistry, Lomonosov Moscow State University, Moscow 119991, Russia

<sup>3</sup> Department of Chemistry, Lobachevsky University, Nizhny Novgorod 603950, Russia

<sup>4</sup> Technology Centre, Mendeleev University of Chemical Technology, 9, Miusskaya Squ., Moscow 125047, Russia

\* Correspondence: pylinina@list.ru

**Abstract:** The effects of NASICON-type phosphates composition on the dehydration of oxygen-containing molecules were probed in reactions of ethanol over double Ti- and Zr-phosphates with rare earth cations  $A_{0.33}M_2(PO_4)_3$  (M – Ti<sup>4+</sup>, Zr<sup>4+</sup>; A – Dy<sup>3+</sup>, Y<sup>3+</sup>, Yb<sup>3+</sup>) at low temperatures (300 – 400°C). The catalysts were characterised via XRD, SEM, BET, and FTIR spectroscopy. Ethylene production was observed on Ti-phosphate, while the formation of diethyl ether (DEE) was observed on Zr-phosphate. The difference in the selectivity of ethanol dehydration is due to the presence of various types of hydroxyl groups characterised by different proton donor mobility depending on the composition of the Ti- and Zr-containing phosphates, which was determined by FTIR analysis of C<sub>6</sub>H<sub>6</sub> adsorption. This work provides a strategy to design highly selective catalysts with framework structure for form-selective reactions with oxygenates considering the location of OH-groups as well as the pore size available for surface intermediates.

**Keywords:** dehydration; diethyl ether; ethylene; Brønsted sites; titanium phosphate; zirconium phosphate; rare-earth elements

## 1. Introduction

Today, the consumption of non-renewable energy sources is responsible for global problems such as increasing greenhouse gas (CO<sub>2</sub>) emissions and the depletion of limited non-renewable resources. The solution to these problems is the use of renewable and sustainable energy sources such as biomass. The conventional fermentation process has long been a commercial success in converting of edible biomass into bioethanol [1]. Driven by the latest innovations, world ethanol production is increasing rapidly. Therefore, it is anticipated that the excess ethanol will become available as a platform molecule for the production of value-added chemicals in the near future. Catalysts and catalytic processes for ethanol conversion to the chemicals such as hydrogen [2] and small oxygenates like acetaldehyde [3,4] and many others [5,6] are widely investigated. The catalytic dehydration of ethanol is a crucial route for producing vital platform chemicals like ethylene and diethyl ether (DEE) [7]. Ethylene is one of the most produced organic compounds in the chemical industry. It is mostly used in the production of polymers (e.g., polyethylene, polyvinylchloride), ethylene oxide, and ethylene glycol, etc. Ethylene is traditionally obtained from petroleum through thermal cracking [8], diethyl ether is a by-product of ethyl alcohol synthesis from ethylene. Diethyl ether is an important

product in the chemical industry, used as an additive in both diesel and petrol engines due to its high volatility, high octane number (over 110), high oxygen content, low auto-ignition temperature, high miscibility with diesel fuel and bioethanol, etc. The catalytic dehydration of bioethanol to ethylene and DEE is an alternative “green” method for their production [9,10]. Many studies have been performed on the dehydration of ethanol, but the search for a stable and selective catalyst for this reaction remains a challenge. The effective catalysts for dehydration reactions include metal oxides [11,12] transition metal triflates [13], Brønsted acids like DBS[14] and heteropoly acids [15]. The nature and density of acidic sites on the catalyst significantly affect selectivity [16]. Strong Brønsted acid sites (BAS) promote dehydration directly to ethylene, while weaker sites may favor the formation of diethyl ether through etherification reactions [17,18]. The presence of Lewis acid sites (LAS) can enhance ethylene selectivity by facilitating the cracking of diethyl ether back to ethanol and ethylene [17]. However, there is only limited insight regarding the reason for the differences in the performance of different acid sites for various types of catalysts. Therefore, it is crucial to gain such understanding and to control the type, strength, and concentration of acid sites on solid acid catalysts for optimized performance for the target products.

NASICON (Na-Super-CONductor)-type catalysts, characterized by their unique framework structure and acid-base properties, have shown promising results in alcohol dehydration reactions [19,20]. The stable 3D framework NASICON structure is constructed through the integration of polyhedra. It consists of “lantern-shaped” units composed of three tetrahedral (e.g.,  $\text{PO}_4$ ) and two octahedral fragments (e.g.,  $\text{ZrO}_6$  or  $\text{TiO}_6$ ). Each unit establishes six connections with other units through the formation of strong covalent bonds. The composition of NASICON-type catalysts can be adjusted by varying metal ions and modifying the framework, allowing for optimization based on specific reaction conditions and desired product selectivity. NASICON-type catalysts are noted for their stability under reaction conditions which is linked to their structural integrity and the ability to maintain active sites during prolonged reactions [21]. The key challenge lies in the regulation of the selectivity of phosphates of complex composition in alcohol transformations. It has been shown that phosphates with 3d metal ions can catalyze the alcohol dehydrogenation reaction [22,23], which can occur on Lewis acid and/or on red-ox sites. Based on the literature [24,25] the prevailing model for complex zirconium phosphates is that the Brønsted acidity originates from hydroxyl groups coordinated to zirconium ( $\text{Zr-OH}$ , strong BAS) and phosphorus ( $\text{P-OH}$ , weak BAS). At the same time, Lewis acidity is attributed to coordinatively unsaturated  $\text{Zr}^{4+}$  ions [26]. In addition to the well-known zirconium phosphates, recent research has focused on titanium phosphates with a framework structure, which also have catalytic properties [21,27]. The activity of complex titanium phosphates in ethylene formation via ethanol dehydration correlates with the strength of the BAS [21]. However, to the best of our knowledge, there is a lack of research evaluating the effect of Ti *via* Zr on the acidity and catalytic activity of NASICON-type phosphates. A comparison of the properties of titanium oxide and zirconium oxide reveals that titanium dioxide typically exhibits higher catalytic activity in dehydration reactions than zirconium dioxide. This enhanced activity can be attributed to the higher density of surface hydroxyl groups, stronger acidity and enhanced hydrophilicity [28–30]. In this work, we reveal the influence of the nature of the framework-forming ion on the activity and selectivity of titanium and zirconium phosphates in the ethanol dehydration reaction, which is sensitive to different types of sites. In addition, the rare-earth elements (REEs) are known to modulate BAS through structural, electronic, and compositional effects, using zeolites widely used as acid catalysts as examples [31,32]. Balancing REE composition and optimizing ion selection (e.g., ionic radius) are critical for tailoring acidity in catalytic applications. Studies have shown a direct correlation between the ionic radius of the REE and the Brønsted acidity of the catalyst. Larger REE ions tend to induce greater changes in the local acid environment, affecting both the number and strength of BAS [33,34]. In consideration of the potential for enhancing the stability of catalysts and optimizing the distribution of products through REE modification, the absence of research focusing on the impact of REE radius in the context of NASICON is a notable gap in the existing literature. The present study involves the doping of Zr-phosphate with a range of rare-earth cations, including

Dy<sup>3+</sup>, Y<sup>3+</sup> and Yb<sup>3+</sup>. A comprehensive investigation has been undertaken to ascertain the influence of REE<sup>3+</sup> radius on the Brønsted acidity, as well as the ethanol dehydration selectivity of these materials.

Ethanol dehydration was chosen as a probe reaction to develop a basic understanding of the effects of the OH-group location within NASICON type phosphate host environments on oxygen removal via dehydration reactions [35]. It provides both confirmative and complementary information regarding the above acidity/basicity-probing methods [36]. Since surface functional groups (OH-groups) and electron acceptor sites play an essential role in the catalytic conversion of alcohols, the adsorption of probe molecules was studied by IR spectroscopy, which provides valuable information on the nature of the active sites.

Therefore, in this study, we report on the role of Brønsted sites in the dehydration of ethanol on titanium and zirconium double phosphates Dy<sub>0.33</sub>M<sub>2</sub>(PO<sub>4</sub>)<sub>3</sub> (M – Zr, Ti), as well as the influence of the nature of the REE on the nature of Brønsted sites and the dehydration capacity of zirconium double phosphates A<sub>0.33</sub>Zr<sub>2</sub>(PO<sub>4</sub>)<sub>3</sub> with REE ions A – Dy, Y, Yb. Fourier transform infrared spectroscopy (FTIR) analysis of CO and C<sub>6</sub>H<sub>6</sub> test-molecules adsorption was used to characterise the surface acid-base properties of the catalysts. Composition–structure–activity of catalysts relationships was discussed.

## 2. Results

### 2.1. Catalysts characterization

#### 2.1.1. Phase Purity and Structure Characterization

The influence of the nature of the ion in the anionic framework has been studied on the example of dysprosium-titanium and dysprosium-zirconium phosphates Dy<sub>0.33</sub>M<sub>2</sub>(PO<sub>4</sub>)<sub>3</sub> with M= Ti<sup>4+</sup>, Zr<sup>4+</sup>. Diffractograms of phosphates are shown in Figure 1a. The X-ray diffraction results of the synthesised samples indicate the formation of NASICON-type phosphates (peaks at 2θ ~ 13,5-14,5°, 20-21°, 23-24°, 28-29°). Titanium and zirconium phosphates belong to the Nasicon-type structure, the precursor of which is NaZr<sub>2</sub>(PO<sub>4</sub>)<sub>3</sub> (NZP). The structure of NaZr<sub>2</sub>(PO<sub>4</sub>)<sub>3</sub> (NZP) is characterized by R $\bar{3}$ c [37] symmetry, for rare earth titanium phosphates the symmetry decreases to R $\bar{3}$  [38]. On the diffractogram of Dy<sub>0.33</sub>Ti<sub>2</sub>(PO<sub>4</sub>)<sub>3</sub> it is indicated by the appearance of peaks at small angles: 2θ = 12,2–12,4° и 12,7–12,8° [39]. For zirconium phosphates A<sub>0.33</sub>Zr<sub>2</sub>(PO<sub>4</sub>)<sub>3</sub> the additional peaks [37] at 2θ = 15,6°; 21,7° and 49,3° can be seen (Figure 1b). It is noted that the reflections of dysprosium-titanium phosphate are shifted to the right relative to dysprosium-zirconium phosphate (Figure 1a), due to the different ionic radius of Ti<sup>4+</sup> и Zr<sup>4+</sup> (0.062 and 0.072 nm, respectively). Differences in the cell parameters of phosphates, as well as in the crystallite sizes, are also related to this fact (Table 1). The radius of the rare earth cation has a weak effect on the lattice parameters for zirconium phosphates.

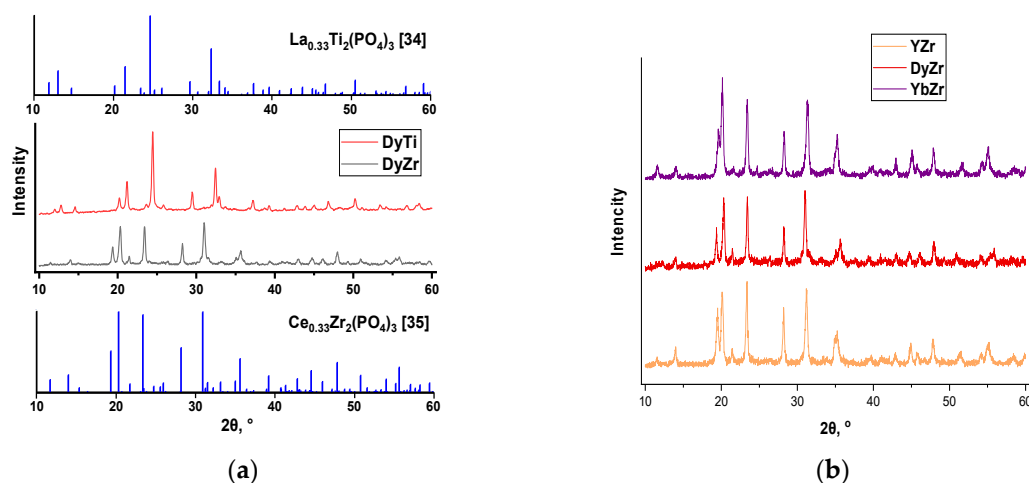


**Figure 1. (a)** XRD patterns of the  $\text{Dy}_{0.33}\text{M}_2(\text{PO}_4)_3$  phosphates where  $\text{M} = \text{Ti}$  (**DyTi**) and  $\text{Zr}$  (**DyZr**); **(b)** XRD patterns of the  $\text{A}_{0.33}\text{Zr}_2(\text{PO}_4)_3$  phosphates where  $\text{A} = \text{Y}^{3+}$  (**YZr**),  $\text{Dy}^{3+}$  (**DyZr**) and  $\text{Yb}^{3+}$  (**YbZr**) simulated basing on the structural data [40,41].

**Table 1.** Lattice parameters of the studied catalysts.

Composition	$r(\text{A}^{3+}), \text{\AA} /$ $r(\text{M}^{4+}), \text{\AA}$	$a, \text{\AA}$	$c, \text{\AA}$	$V, \text{\AA}^3$	$r, \text{nm}^1$
<b>DyZr</b>	0.912 / 0.72	8.823(2)	22.65(7)	1527	30
<b>YZr</b>	0.90 / 0.72	8.826(2)	22.57(2)	1525	32
<b>YbZr</b>	0.868 / 0.72	8.829(3)	22.53(1)	1510	27
<b>DyTi</b>	0.912 / 0.61	8.357(1)	21.98(1)	1330	28

<sup>1</sup>  $r(\text{A}^{3+}), \text{\AA} / r(\text{M}^{4+}), \text{\AA}$  – Shannon ionic radii of metals. <sup>2</sup> Calculated by Sherer equation.

The IR spectra of  $\text{Dy}_{0.33}\text{M}_2(\text{PO}_4)_3$  with  $\text{M} = \text{Zr}^{4+}, \text{Ti}^{4+}$ , showed absorption bands related to the vibrations of the  $\text{PO}_4$  group (Figure 2) in the range from 500 to 650  $\text{cm}^{-1}$  - asymmetric bending vibrations, from 900 to 1000  $\text{cm}^{-1}$  - symmetric stretching vibrations and from 1000 to 1280  $\text{cm}^{-1}$  - asymmetric stretching vibrations [42]. The maximum number of vibration bands allowed by the selection rules is: six bands of stretching (1210-1010  $\text{cm}^{-1}$ ) and bending asymmetric vibrations (650-540  $\text{cm}^{-1}$ ), two bands of stretching (1010-900  $\text{cm}^{-1}$ ) and four bands of bending symmetric vibrations (<500  $\text{cm}^{-1}$ ), but due to the partial overlapping of closely located bands, their distinguishable number in the spectra could be less than these values. The IR spectrum of  $\text{Dy}_{0.33}\text{Zr}_2(\text{PO}_4)_3$  has a higher number of bands compared to the IR spectrum of  $\text{Dy}_{0.33}\text{Ti}_2(\text{PO}_4)_3$ , which is due to the fact that theoretically, compounds with the space group  $\text{P}\bar{3}\text{c}$  are characterised by seven or eight asymmetric stretching vibrational bands instead of six, which is characteristic of the space group  $\text{R}\bar{3}$  [43].

Thus, according to the results of X-ray phase analysis and IR spectroscopy, the sample  $\text{Dy}_{0.33}\text{Ti}_2(\text{PO}_4)_3$  has the space group  $\text{R}\bar{3}$  and the sample  $\text{Dy}_{0.33}\text{Zr}_2(\text{PO}_4)_3$  has  $\text{P}\bar{3}\text{c}$ . The nature of the REE ion has virtually no effect on the spectra of zirconium phosphate (Figure S1).

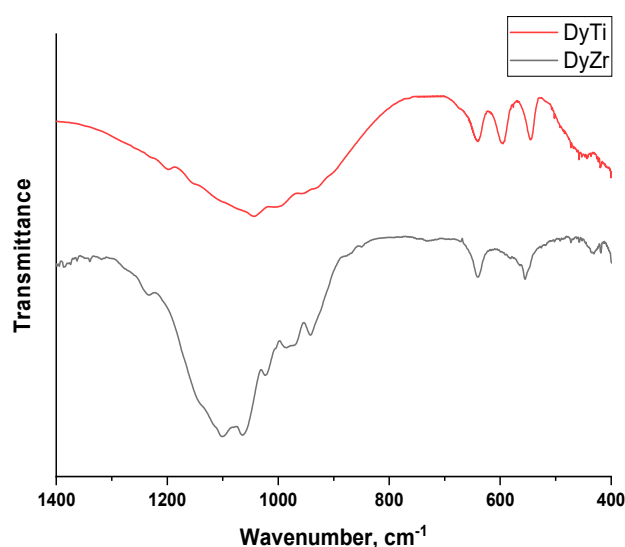


**Figure 2.** IR spectra of the  $\text{Dy}_{0.33}\text{M}_2(\text{PO}_4)_3$  phosphates where  $\text{M} = \text{Ti}$  and  $\text{Zr}$ .

### 2.1.2. Surface and Porosity Characterization

The scanning electron microscope (SEM) images in Figure 3 show that Zr-phosphate particles of about 100 nm have a more "ordered" shape similar to spheres, while Ti-phosphate is characterized by larger particles of highly aggregated irregularly shaped particles.

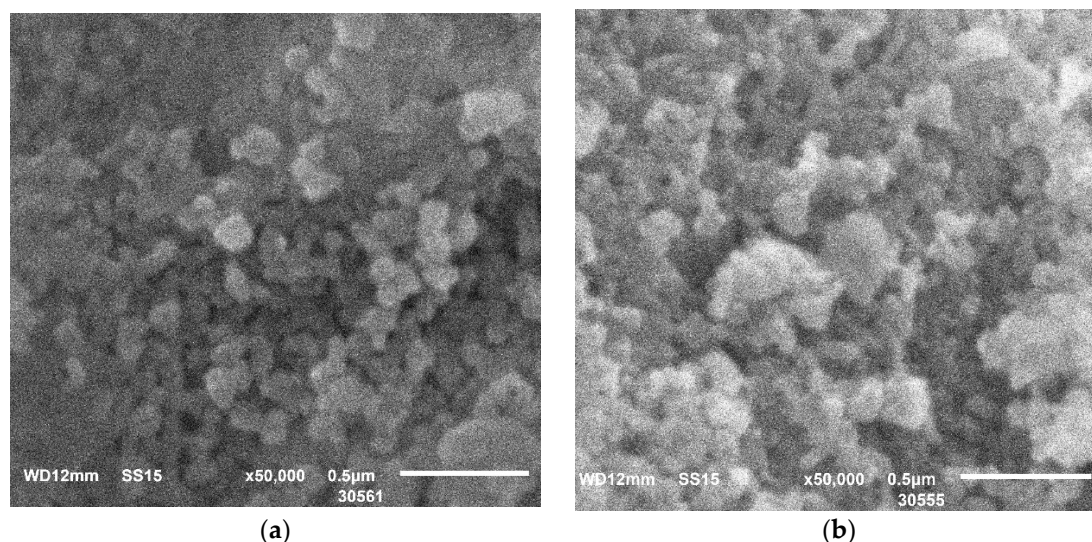


**Figure 3.** Scanning electron image of the compounds: (a)  $\text{Dy}_{0.33}\text{Zr}_2(\text{PO}_4)_3$ ; (b)  $\text{Dy}_{0.33}\text{Ti}_2(\text{PO}_4)_3$ .

Figure 4 shows the  $\text{N}_2$  adsorption-desorption isotherms of the investigated catalysts. The isotherms are a combination of type III and type V, with a type H3 hysteresis according to the IUPAC definition; this indicates the presence of both mesopores and macropores and is in accordance with [21]. The composition of the samples has a marked effect on the porous characteristics (Table 2). Titanium phosphate  $\text{Dy}_{0.33}\text{Ti}_2(\text{PO}_4)_3$  has a larger specific surface area (BJH), volume and pore diameter than zirconium phosphate  $\text{Dy}_{0.33}\text{Zr}_2(\text{PO}_4)_3$  (Table 2). These differences are specifically related to the porous structure of the samples, as the BET surface of these samples is the same. For zirconium phosphates with different REE ions, the sample with the smaller ion radius (YZr) has the largest surface area (both BET and BJH).

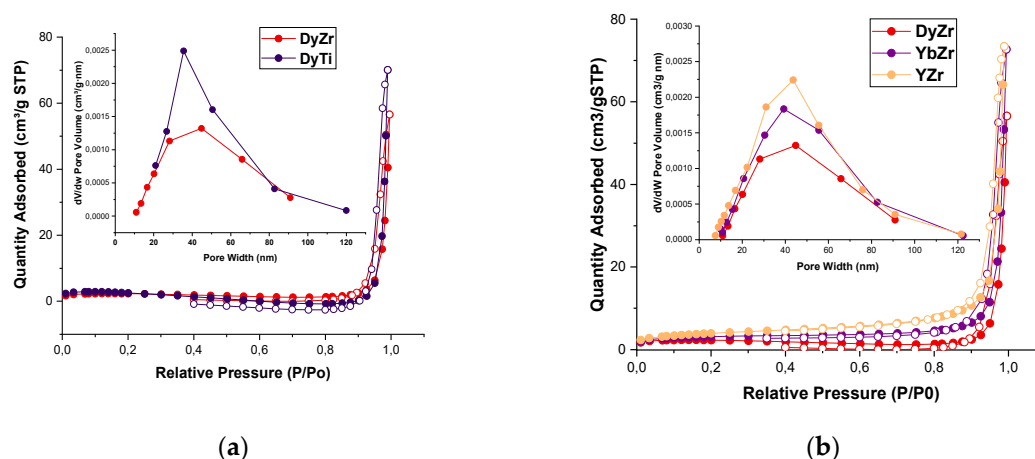


**Figure 4.** Nitrogen adsorption–desorption isotherms and pore size distributions of (a) the  $\text{Dy}_{0.33}\text{Zr}_2(\text{PO}_4)_3$  (DyZr) and  $\text{Dy}_{0.33}\text{Ti}_2(\text{PO}_4)_3$  (DyTi) compounds; (b) the  $\text{A}_{0.33}\text{Zr}_2(\text{PO}_4)_3$  compounds where  $\text{A} = \text{Y}^{3+}$  (YZr),  $\text{Dy}^{3+}$  (DyZr) and  $\text{Yb}^{3+}$  (YbZr).

**Table 2.** Surface area and porous characteristics of the compounds Dy<sub>0.33</sub>M<sub>2</sub>(PO<sub>4</sub>)<sub>3</sub> with M= Ti<sup>4+</sup> and Zr<sup>4+</sup>.

Composition	BET Surface (m <sup>2</sup> /g)	BJH Surface (m <sup>2</sup> /g)	Pore Volume (cm <sup>3</sup> /g)	Average Pore Diameter (nm)	Most Probable Pore Diameter (nm)
DyTi	7,0	10,0	0,11	44	36
DyZr	7,1	7,6	0,08	41	45
YbZr	10,6	10,1	0,11	45	39
YZr	13,9	11,3	0,11	40	44

2.1.3. Acid-Base Properties

The electron-acceptor and proton-donor surface properties of the samples were investigated using Fourier transform infrared spectroscopy (FTIR) with to analyse the adsorption of CO [44–46] и C<sub>6</sub>H<sub>6</sub> [47] as probe molecules. The formation of a donor-acceptor complex between CO and an aprotic center involves electron transfer from the antibonding 5σ-orbital to the cation’s vacant orbital, leading to an increase in the CO vibrational frequency [44]. Previously, the infrared spectroscopic studies of CO and benzene adsorption in ternary aluminium-titanium-phosphates have been described [21].

FTIR spectra of adsorbed CO on titanium and zirconium double phosphates were indicating the absence of Lewis acid centers on the surface, which may be related to the inaccessibility of rare element cations during surface reconstruction under thermal vacuum treatment conditions. This result agrees with the data obtained earlier for double nickel-titanium and manganese-titanium phosphates FTIR [21].

As is well known [44], the phosphates possess the three types of OH-groups that correspond to the absorption bands at 3743–3745, 3697–3711 and 3663–3678 cm<sup>-1</sup>. These bands can be attributed to the Brønsted acid sites (BASs). According to the classification of hydroxyl groups given in[44,48], the bands are attributed to the various surface OH groups which differ in their coordination of surrounding metal atoms. These groups are acting as Brønsted acid sites (BASs). Type I is attributed to terminal hydroxyl groups (one-coordinated), type II to bridging (bi-coordinated), and type III to tri-coordinated surface OH groups (Figure S2). An increase in the number of surrounding cations strengthens the proton-donating ability of the OH-group, which in turn defines the Brønsted acid site strength.

The spectra of zirconium-phosphates are characterised by the presence of several bands for the same type of hydroxyls - 3764, 3742 cm<sup>-1</sup> for terminal and 3670, 3646 cm<sup>-1</sup> for tri-coordinated hydroxyls. A single band, 3698 cm<sup>-1</sup>, is observed for bridging (bi-coordinated) ones. For titanium phosphate Dy<sub>0.33</sub>Ti<sub>2</sub>(PO<sub>4</sub>)<sub>3</sub> there is no such effect and the bands are single - 3744 cm<sup>-1</sup> terminal, 3702 cm<sup>-1</sup> bridging (bi-coordinated), 3671 cm<sup>-1</sup> tri-coordinated (Table 3, Figure S3).

The strength of BASs was characterized by “proton affinity” (PA). In the case of acids, the PA is determined by the enthalpy (ΔH) of the proton transfer reactions between the acid and the acid residue [47]. We can use the PA to characterise the interaction of acidic OH groups of the surface with base molecules in the gas phase. The weak hydrogen bonding method can be used to determine PA [47] with benzene as probe molecules. The magnitude of the shift of the OH-group vibrational frequency during the formation of the H-complex with benzene correlates with the proton-donating ability of the OH-group – the greater the shift, the higher the proton-donating ability and the lower the value of PA. The FTIR spectrum of C<sub>6</sub>H<sub>6</sub> adsorption on double titanium- and zirconium phosphates and the difference spectra of the sample after and before benzene adsorption are shown in Figure S3, Figure S4. The data obtained are shown in Table 3.

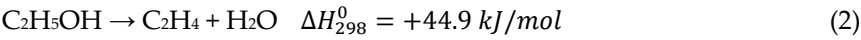
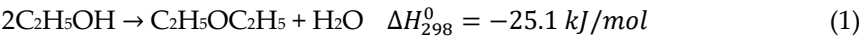
Table 3. Acidic characteristics of the catalysts.

Sample	$\nu(\text{OH}), \text{cm}^{-1}$	Type	$\nu(\text{OH}\cdots\text{H}), \text{cm}^{-1}$	$\Delta\nu, \text{cm}^{-1}$	PA, kJ/mol
DyTi	3744	I	3602	142	1341
	3702	II	3555	147	1334
	3671	III	3461	210	1266
DyZr	3764	I	3602	162	1316
	3742	I	3602	140	1344
	3698	II	3550	148	1333
	3670	III	3478	192	1283
	3646	III	3478	168	1309
YbZr	3769	I	3602	167	1310
	3743	I	3602	141	1342
	3695	II	3560	135	1351
	3671	III	3478	193	1282
	3644	III	3478	166	1311
YZr	3768	I	3602	166	1311
	3744	I	3602	142	1341
	3696	II	3566	130	1358
	3668	III	3471	197	1278

The largest band shift after benzene adsorption was observed for type III sites (Brønsted acid site). In addition, the shift for the  $\text{Dy}_{0.33}\text{Zr}_2(\text{PO}_4)_3$  sample ( $192 \text{ cm}^{-1}$ ) is smaller than that for the  $\text{Dy}_{0.33}\text{Ti}_2(\text{PO}_4)_3$  ( $210 \text{ cm}^{-1}$ ). Proton affinity values, which characterise the energy of proton (hydrogen ion) binding to a molecule or ion in the gas phase, were calculated from the data presented. The PA energy (proton affinity) of type III hydroxyls for zirconium phosphate is  $1283 \text{ kJ/mol}$ , while for titanium phosphate it is lower at  $1266 \text{ kJ/mol}$ . Thus, the proton-donating properties are higher for  $\text{Dy}_{0.33}\text{Ti}_2(\text{PO}_4)_3$  than for  $\text{Dy}_{0.33}\text{Zr}_2(\text{PO}_4)_3$ . The shifts and PA energy values of type I and II hydroxyls for the studied samples differ insignificantly. In the case of zirconium phosphates with REE, the RA energy value for terminal OH-groups of Zr-OH increases in the  $\text{Yb} \rightarrow \text{Y} \rightarrow \text{Dy}$  series, implying a decrease in the proton donor mobility. For bridging hydroxyls, the proton donating ability increases in the series  $\text{Y} \rightarrow \text{Yb} \rightarrow \text{Dy}$  and for three-coordinated hydroxyls in the series  $\text{Yb} \rightarrow \text{Dy} \rightarrow \text{Y}$ .

2.2. Catalytic Ethanol Dehydration

Studied samples were tested in the gas-phase conversion of ethanol, which can proceed in the following directions: formation of ethylene (E) and diethyl ether (DEE) via dehydration reactions and formation of acetaldehyde (AcH) via a dehydrogenation reaction. In our case, dehydration reactions were observed with the formation of ethylene and diethyl ether [49]:



The thermodynamically favorable product is DEE at low temperatures and ethylene at high temperatures [50].

Figure 5 shows the temperature dependence of alcohol conversion and process selectivity on  $\text{Dy}_{0.33}\text{M}_2(\text{PO}_4)_3$  framework phosphates, with  $\text{M} = \text{Zr}, \text{Ti}$ . The maximum ethanol conversion was observed on the  $\text{Dy}_{0.33}\text{Ti}_2(\text{PO}_4)_3$  sample:  $W=48\%$  at  $T= 400^\circ\text{C}$ . On titanium phosphate DyTi the selectivity for ethylene increased with increasing temperature and the selectivity for diethyl ether

decreased, whereas on zirconium phosphate diethyl ether was the main reaction product over the whole temperature range (Figure 5b). Acetaldehyd was formed in insignificant amounts, its yield did not exceed 5 %.

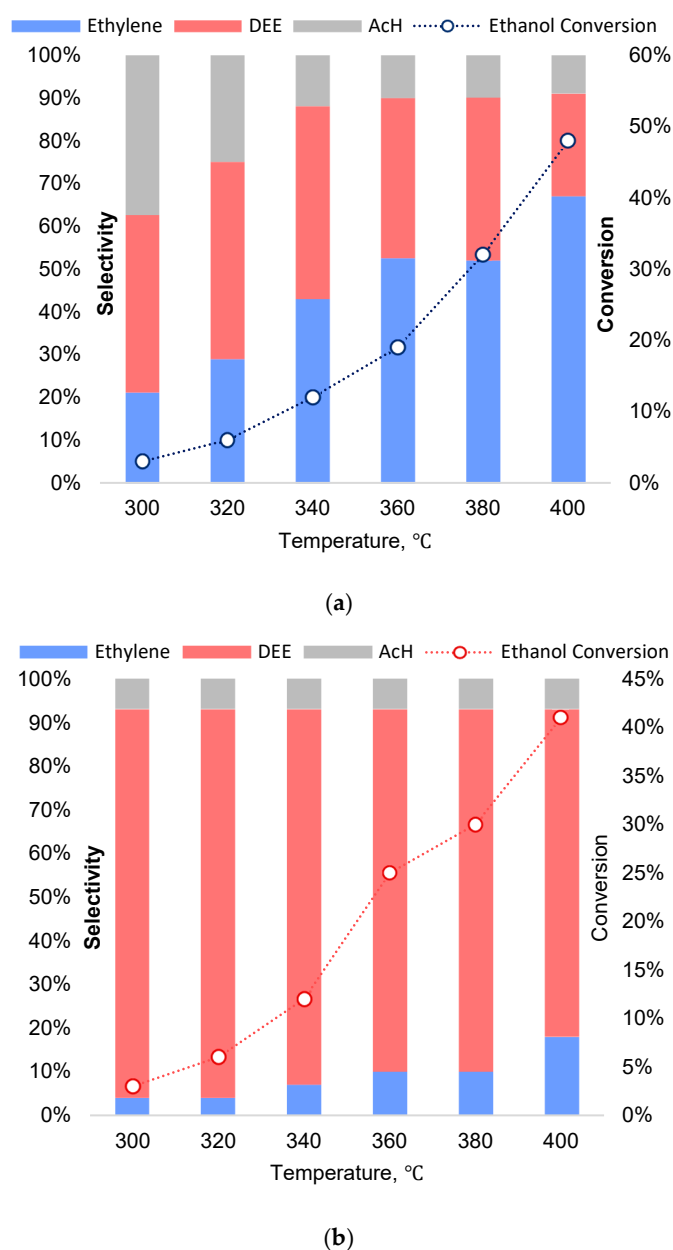


**Figure 5.** The ethanol conversion and the selectivity of the reaction products on the (a) DyTi and (b) DyZr catalysts.

In the case of zirconium phosphates, the maximum ethanol conversion was observed for the  $Y_{0.33}Zr_2(PO_4)_3$  sample ( $W=45\%$ ) and the minimum for the  $Yb_{0.33}Zr_2(PO_4)_3$  sample ( $W=37\%$ ), while the selectivity towards diethyl ether for the ytterbium sample was maximum at 81% at 400°C (Figure 6, Figure S5).

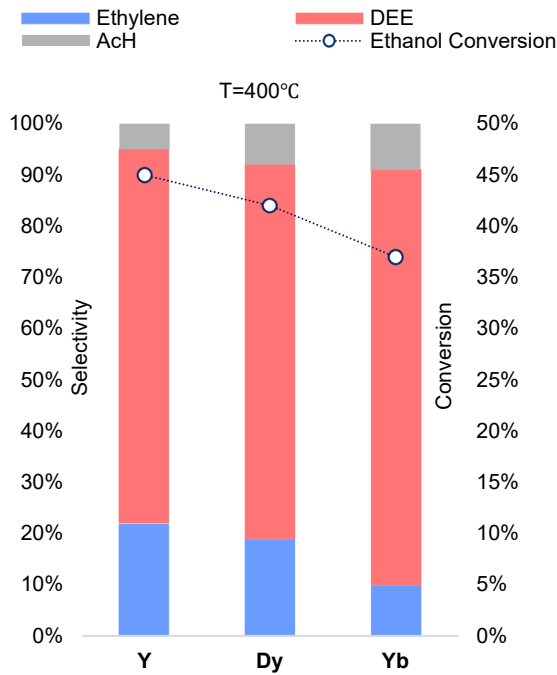


**Figure 6.** The ethanol conversion and the selectivity of the reaction products on the  $A_{0.33}Zr_2(PO_4)_3$  compounds where A= Y, Dy and Yb.

Differences in the catalytic activity (selectivity) of ethanol dehydration are related to the nature of the acid centers of the phosphate surface therefore to the nature of the framework cation (Ti or Zr). To a lesser extent, as can be seen from the data obtained, they are related to the nature of the REE in the cationic part of the phosphate. It is also confirmed by the values of the experimental activation energies of the intra- and intermolecular dehydration reactions of ethanol (Table 3, Figure S6).

**Table 3.** Apparent activation energy and pre-exponential factor of the  $A_{0.33}M_2(PO_4)_3$  (M – Ti, Zr; A – Dy, Y, Yb) catalysts.

Sample	Ea, kJ·mol <sup>-1</sup>		lnN	
	Ethylene	DEE	Ethylene	DEE
DyTi	119	80	18.3	10.8
DyZr	139	95	20.4	14.5
YZr	128	100	18.8	15.4
YbZr	140	104	20.0	15.8

The highest ethylene selectivity as observed on YZr, which is consistent with the lowest values of activation energy of intramolecular dehydration of ethanol compared to DyZr and YbZr samples. The highest selectivity of DyZr towards diethyl ether is due to the lowest activation energy of intermolecular dehydration compared to YbZr and YZr.

Table 4 shows a comparison of recently published catalysts for alcohol dehydration. As can we see, zeolites remain a benchmark for alcohol dehydration due to their strong acidity and good alkene selectivity but suffer from coking and stability issues. Aluminosilicates and NASICON-type phosphates offer a promising alternative with stable performance and resistance to coke formation

**Table 4.** Performance of various catalysts for ethanol dehydration.

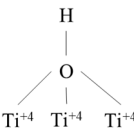
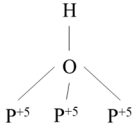
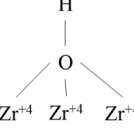
Catalyst Composition	Conditions	Ethanol Conversion	Selectivity to Ethylene	Selectivity to DEE	Reference(s)
YbZr	T = 380°C	37	10	81	This work
DyTi	T = 400°C	48	67	24	This work
LaTi	T = 380°C	20	37	45	[51]
MnTi	T = 380°C	50	40	22	[21]
Zr/HZSM-5	T = 450°C	100	61	-	[52]
SAPO-34	T = 400°C	92	52	1	[53]
SAPO-11	T = 340°C	95	91	9	
Zn-SAPO-11	T = 340°C	85	15	-	
WO <sub>3</sub> -ZrO <sub>2</sub>	T = 400°C	100	100	-	[54]
MoO <sub>3</sub> -ZrO <sub>2</sub>	T = 380°C	98	69	-	
NA/HZSM-5(12)	T = 200°C	10	2	98	[55]
	T = 300°C	95	98	2	
$\gamma$ -Al <sub>2</sub> O <sub>3</sub>	T = 200°C	26.9	0.6	99.4	[56]
	T = 400°C	100	98	0	
La- $\gamma$ -Al <sub>2</sub> O <sub>3</sub>	T = 200°C	18	0.5	99.5	
	T = 400°C	100	96.6	0.1	
5Al <sub>2</sub> O <sub>3</sub> -95ZrO <sub>2</sub>	T = 340°C	12	10	15	[36]
	T = 380°C	20	45	20	

3. Discussion

Differences in the catalytic activity (selectivity) of ethanol dehydration are related to the nature of the acid sites (AS) on the surface of titanium. The formation of ethylene is known to occur through the formation of an ethoxy group upon adsorption of ethanol onto the strong acid sites of both Lewis and Brønsted [57]. It is also known that the presence of basic sites on the surface facilitates the adsorption of the alcohol molecule. At the same time, the ethoxy group is thought to be an intermediate in the formation of diethyl ether [58]. DEE can be formed by coordination of an ethoxy group formed on the acid site and an ethanol molecule adsorbed on the basic site. Another mechanism of DEE formation involves the coordination of an ethylene molecule already formed on the strong Lewis acid site, which acts as an intermediate for DEE formation [57]. In addition, *Hsu Chiang et al.* [35] reported that Brønsted acid sites located in small side pockets in zeolites could protect ethanol monomers against the formation of ethanol dimers because of size exclusion; hence, it can selectively catalyze the unimolecular dehydration of ethanol to ethylene.

The occurrence of predominantly intramolecular dehydration with ethylene formation on titanium phosphate, DyTi, indicates the presence of a strong acid site on its surface. According to FTIR data, a three-coordinated OH-group with high proton donor mobility can act as such a site. Considering that the DEE formation reaction also occurs in this sample, it can be assumed that the formation of the product from the ethoxy group is determined by the thermodynamics of the process. DEE is formed at low temperatures by the addition to the ethoxy group of another ethanol molecule coordinated at the main site, which may be the terminal OH-group (P-OH), the presence of which is confirmed by FTIR methods. At high temperatures, ethylene is formed from the ethoxy group (Table 5).

**Table 5.** Catalytic consequences of hydroxyl group location on the pathways of dehydration reactions.

Sample	Type of OH-group		Main product <i>via</i> ethanol dehydration
	I	III	
DyTi	P-OH		Ethylene
DyZr	P-OH		DEE
	Zr-OH		

On zirconium phosphate, DyZr, the intermolecular dehydration reaction is the main reaction over the entire temperature range and the DEE yield also increases at high temperatures. The predominant intermolecular dehydration requires the presence of an acid site on the catalyst surface for the formation of the ethoxy group (or for the coordination of ethylene in the case of Lewis acid sites) and the basic site for the coordination of the ethanol molecule located near the acid site for the formation of the DEE molecule. Analysis of benzene adsorption data on the surface of Dy<sub>0.33</sub>Zr<sub>2</sub>(PO<sub>4</sub>)<sub>3</sub> indicates the presence of two kinds of three-coordinated OH-groups, which play the role of acid sites, and two kinds of terminal OH-groups (P-OH, Zr-OH). It should be noted that there is an additional band at low frequencies (3646 cm<sup>-1</sup>) on zirconium phosphate, corresponding to a three-coordinated OH-group, which is not observed on titanium phosphate, allowing it to be attributed to the OH-group three-coordinated with phosphorus. Dy<sub>0.33</sub>Zr<sub>2</sub>(PO<sub>4</sub>)<sub>3</sub> is characterised by the presence of an additional band also in the region of the terminal OH-groups (3764 cm<sup>-1</sup>), which is not observed in Dy<sub>0.33</sub>Ti<sub>2</sub>(PO<sub>4</sub>)<sub>3</sub> and can be attributed to Zr-OH. Thus, the bands in zirconium phosphate at 3764 and 3742 cm<sup>-1</sup> are attributed to the terminal hydroxyls of Zr-OH and P-OH, respectively. This means that unlike Dy<sub>0.33</sub>Ti<sub>2</sub>(PO<sub>4</sub>)<sub>3</sub>, which has predominantly strong BASs (three-coordinated), Dy<sub>0.33</sub>Zr<sub>2</sub>(PO<sub>4</sub>)<sub>3</sub> has both acidic and basic sites (three-coordinated and terminal, respectively) on its surface. In addition, the proton donor capacity of the acid sites in zirconium phosphate is lower than in titanium phosphate. All this allows us to explain the formation of DEE on Dy<sub>0.33</sub>Zr<sub>2</sub>(PO<sub>4</sub>)<sub>3</sub> over the whole temperature range of the reaction. To produce diethyl ether, one molecule of ethanol is activated as an ethoxy group on a three-coordinated OH-group (Table 4). The possibility of the ethoxy group interacting with the second ethanol molecule is conditioned by the presence of an additional terminal OH-group and the longer bond length of Zr-O (~2.1 Å) than Ti-O (~1.9 Å) [41,51]. In addition, our data show that the proton donor mobility, which favours the formation of ethoxy groups, is higher in titanium phosphate, which is consistent with the lower activation energy of ethylene formation (Table 3). The Ea value of DEE formation on titanium phosphate is also lower than that on zirconium phosphate, confirming our conclusion that the ethoxy group is also involved in DEE formation (Table 3).

Differences in the selectivity of ethanol dehydration are also due to differences in the porous characteristics of titanium- and zirconium-phosphates. Our results clearly show that bimolecular dehydration of ethanol preferentially occurs in large pore zirconium phosphates (Table 2).

When considering the influence of the nature of the REE in zirconium phosphates on the pathway of the ethanol dehydration reaction, the regularities described above are also observed. On

the YZr sample there are three-coordinated Brønsted sites with the highest proton donating ability, responsible for the formation of the ethoxy group, followed by the formation of the ethylene molecule. The highest selectivity towards diethyl ether on the  $\text{Dy}_{0.33}\text{Zr}_{1.67}(\text{PO}_4)_3$  sample is due to the presence of acidic Brønsted sites (type III) with moderate proton donating ability and the simultaneous presence of strong basic Brønsted sites (type I) with low proton donating ability (Table 2). With increasing proton donor mobility, the three-coordinated hydroxyls  $\text{Yb} \rightarrow \text{Dy} \rightarrow \text{Y}$  have an increased selectivity for ethylene, which is consistent with a decrease in the activation energy of the intramolecular ethanol dehydration reaction. It should be noted that the decrease of the proton donating ability of the terminal hydroxyls (basic sites) on the studied zirconium phosphates  $\text{Yb} \rightarrow \text{Y} \rightarrow \text{Dy}$  increases the selectivity towards diethyl ether, which is also in accordance with the decrease of the activation energy of the intermolecular ethanol dehydration.

## 4. Materials and Methods

### 4.1. Synthesis of the Catalysts

The samples were synthesized using the following reagents from LLC “Vecos”:  $\text{A}_2\text{O}_3$  (A – Dy, Y, Yb; purity >99.9%)  $\text{ZrOCl}_2 \cdot 8\text{H}_2\text{O}$  (>99.0%),  $\text{NH}_4\text{H}_2\text{PO}_4$  (>99.5%), aqueous solutions of  $\text{TiCl}_3$  (15%)  $\text{NH}_3$ ,  $\text{HCl}$  (35–38%),  $\text{HNO}_3$  (65%), citric acid monohydrate  $\text{C}_6\text{H}_8\text{O}_7 \cdot \text{H}_2\text{O}$  (>99.8%), and ethylene glycol  $\text{C}_2\text{H}_6\text{O}_2$  (>99.8%).  $\text{A}_2\text{O}_3$  powders were dissolved in nitric acid, while  $\text{NH}_4\text{H}_2\text{PO}_4$  was dissolved in distilled water. The  $\text{TiOCl}_2$  solution was prepared by oxidizing 15%  $\text{TiCl}_3$  (aq.) with concentrated  $\text{HCl}/\text{HNO}_3$  under ambient conditions, followed by gravimetric concentration analysis.  $\text{ZrOCl}_2$  concentration was similarly determined.

Zirconium-containing phosphates were synthesized via sol-gel method. The procedure was similar to the described in [59]. A stoichiometric  $\text{Dy}(\text{NO}_3)_3/\text{ZrOCl}_2$  mixture was combined with  $\text{NH}_4\text{H}_2\text{PO}_4$  solution. The product was dried at 90°C (48 h) and 130°C (48 h), followed by calcination at 600–750°C (48–72 h per step) with intermediate grinding.

Titanium phosphate could not be obtained by the conventional sol-gel method without the use of organic reagents, so the Pechini method was used to synthesize it. The synthesis methodology is described in [51]. Stoichiometric  $\text{Dy}(\text{NO}_3)_3$  and  $\text{TiOCl}_2$  solutions were mixed at 60°C. Citric acid (15:1 molar ratio to total metal ions) was added, followed by ethylene glycol (4:1 to metal ions) and  $\text{NH}_4\text{H}_2\text{PO}_4$  under stirring. The gel was dried stepwise at 90°C (48 h), 130°C (48 h), and 350°C (4 h), then calcined sequentially at 500–670°C (48–72 h per step). The samples were note as **DyZr**, **YZr**, **YbZr**.

### 4.2. Characterization of the Catalysts

Phase composition was analyzed via X-ray diffraction (XRD, Shimadzu XRD-6000,  $\text{CuK}\alpha$  radiation,  $2\theta = 10\text{--}60^\circ$ ,  $1^\circ/\text{min}$ ). Patterns were indexed using structural analogs [40,41].

Low temperature nitrogen physisorption isotherms were recorded on a «TriStar-3020 (Norcross, GA 30093, USA)» Surface Area and Porosity Analyzer after the samples were degassed in a vacuum at 200°C for 5 h. Then, the Brunauer–Emmett–Teller (BET) model was applied to calculate the specific surface area, and the pore-size distribution was calculated using the Barrett–Joyner–Halenda (BJH) model.

Scanning electron microscopy (SEM) images were taken on the EVO-40 scanning electron microscope (Carl Zeiss, Jena, Germany).

The adsorption properties (Lewis acidity) of the samples were measured by diffuse reflectance FTIR spectroscopy with an EQUINOX 55/S instrument (Bruker, Billerica, MA, USA). The powdered sample was placed in a quartz cell with a  $\text{CaF}_2$  window and calcined at 550 °C for 1 h on air, and then calcined for 2 h under a vacuum ( $p < 5 \cdot 10^5$  Torr).

After that, the background spectrum was recorded. To determine the Lewis acidity of the supports, the adsorbed CO spectra were recorded at room temperature and at 5, 20 and 50 Torr pressures. The differential spectra of the adsorbed CO were obtained by subtracting the background

spectrum from the experimental spectrum, followed by the correction of the baseline in an OPUS 6.0 software (Bruker, Billerica, MA, USA). High-purity carbon monoxide (>99.9) was further cleaned by passing it through a liquid nitrogen trap and storing it over calcined molecular sieves. The Brønsted sites were obtained from the IR spectra by the H-bond method, with benzene as spectral probe. This procedure made it possible to measure the concentration and strength of the Brønsted acid sites (BASs).

The strength of the BASs was characterized by proton affinity (PA), that is, the energy of proton detachment from the surface OH group, which was calculated in accordance with the procedure described in [60].

#### 4.3. Catalytic Tests

Catalytic experiments were performed at atmospheric pressure in a tubular flow reactor (i.d. 6 mm) using a 0.03 g catalyst and feeding ethanol in argon; it had a total flow rate of 1.2 L/h). The carrier gas (argon) was passed through a bubbler containing ethanol (97%), maintained at a constant temperature (25 °C), in order to obtain the desired partial pressures. The temperature in the experiment was varied stepwise from 300 to 400 °C. The outlet gases were analyzed by a Chromatec-Crystal 5000 (Chromatec, Yoshkar-Ola, Russia) gas chromatograph (GC), equipped with a “Parapak Q” column and TCD and FID detectors.

### 5. Conclusions

In the work presented, the titanium and zirconium phosphates with rare earth cations  $A_{0.33}M_2(PO_4)_3$  ( $M = \text{Ti, Zr}$ ;  $A = \text{Dy, Y, Yb}$ ) have been synthesized and characterized. They are shown to be crystallized in the NASICON type framework structure with ordered occupation of the cavities by rare earth  $M^{3+}$  cations. It is found that the nature of the framework-forming ion ( $M = \text{Zr, Ti}$ ) determines the lattice symmetry: zirconium phosphates (ZrP) crystallise in  $P\bar{3}c$  symmetry and titanium phosphates (TiP) in  $R\bar{3}$ .

Ethanol dehydration reactions on double zirconium and titanium phosphates at 300 – 400 °C showed that titanium phosphate was found to be able to catalyze the conversion of ethanol to both ethylene and diethyl ether, while zirconium phosphate could predominantly catalyze only bimolecular reactions of ethanol dehydration to diethyl ether. Differences in ethanol conversion selectivity are related to the localisation of the hydroxyl groups in the phosphate framework. FTIR analysis of the  $C_6H_6$  adsorption revealed the presence of several types of OH-groups, characterised by different proton-donor mobility. The formation of ethylene was found to occur on acidic Brønsted sites (BASs) (with high proton donor mobility), and the formation of diethyl ether - on moderate strength BASs and basic sites of terminal OH-groups. It is shown that the experimental activation energy of the intramolecular dehydration of ethanol decreases as the proton-donating mobility of three-coordinated hydroxyls (BASs) increases, whereas the activation energy of the intermolecular dehydration of ethanol decreases as the proton-donating ability of terminal OH-groups decreases.

Thus, the results show that the design and selection of micro- and mesoporous porous catalysts with framework structure for form-selective reactions with oxygenates should consider the location of OH-groups as well as the pore size available for surface intermediates.

**Supplementary Materials:** The following supporting information can be downloaded at the website of this paper posted on Preprints.org., Figure S1: IR spectra of the  $A_{0.33}Zr_2(PO_4)_3$  phosphates where  $A = Y^{3+}$ ,  $Dy^{3+}$  and  $Yb^{3+}$ ; Figure S2: The types of OH-groups on the surface; Figure S3: Different diffuse reflectance infrared Fourier transform spectra at room temperature: (a) for initial surface of DyZr; (b) for the surface of DyZr with adsorbed  $C_6H_6$ ; (c) for initial surface of DyTi; (d) for the surface of DyTi with adsorbed  $C_6H_6$ ; (e) for initial surface of YZr; (f) for the surface of YZr with adsorbed  $C_6H_6$ ; (g) for initial surface of YbZr; (h) for the surface of YbZr with adsorbed  $C_6H_6$ ; Figure S4: Difference diffuse reflectance infrared Fourier transform spectra of the sample after and before benzene adsorption: (a) DyTi; (b) DyZr; (c) YZr; (d) YbZr; Figure S5: Ethanol conversion (a) and

ethylene (b) and DEE (c) yields over Zr-phosphates  $A_{0.33}Zr_2(PO_4)_3$  with  $A = Y, Dy, Yb$ ; Figure S6: Arrhenius plots for DEE formation (yellow) and ethylene formation (blue) over (a)  $Dy_{0.33}Zr_2(PO_4)_3$ , (b)  $Dy_{0.33}Ti_2(PO_4)_3$ .

**Author Contributions:** For research articles with several authors, a short paragraph specifying their individual contributions must be provided. The following statements should be used “Conceptualization, A.Z. and A.K.; methodology, A.Z., A.K., E.A.; validation, A.Z., A.K., E.A., V.P.; formal analysis, A.K., A.S., D.O., D. Z., Y.F.; investigation, A.Z., A.S., E.A., E.F., V.S., V.Pr., A.K., D.O., D. Z., Y.F.; resources, A.Z., E.A., A.K.; data curation, A.Z., A.S., E.A., V.S., V.Pr., A.K., Y.F.; writing—original draft preparation, A.Z., E.A., A.K., Y.F., D.O., I.M.; writing—review and editing, A.Z., A.K., E.A., V.P.; visualization, A.Z., A.S., A.K.; supervision, A.Z.; project administration, A.Z. All authors have read and agreed to the published version of the manuscript.”

**Funding:** The work was carried out with the financial support of the Ministry of Education and Science of the Russian Federation (the basic part of the state task, the project № FSWR-2023-0025) (Elena A. Asabina)

**Data Availability Statement:** Data will be available from the corresponding author upon reasonable request.

**Acknowledgments:** The authors acknowledge support from Lomonosov Moscow State University Program of Development for FTIR spectroscopy analysis (MSU Chemistry Department “Nano chemistry and the Nanomaterials” Equipment Center). The authors express their gratitude to the D.I. Mendeleev Center for the collective use of scientific equipment for assistance in carrying out SEM and BET researches.

**Conflicts of Interest:** The authors declare no conflicts of interest.

## References

1. Sun, J.; Wang, Y. Recent Advances in Catalytic Conversion of Ethanol to Chemicals. *ACS Catal* **2014**, *4*, 1078–1090, doi:10.1021/cs4011343.
2. Chen, W.H.; Biswas, P.P.; Ong, H.C.; Hoang, A.T.; Nguyen, T.B.; Dong, C. Di A Critical and Systematic Review of Sustainable Hydrogen Production from Ethanol/Bioethanol: Steam Reforming, Partial Oxidation, and Autothermal Reforming. *Fuel* **2023**, *333*, doi:10.1016/j.fuel.2022.126526.
3. Zhukova, A.; Chuklina, S.; Fionov, Y.; Vakhrushev, N. Enhanced Ethanol Dehydrogenation over Ni - Containing Zirconia - Alumina Catalysts with Microwave - Assisted Synthesis. *Research on Chemical Intermediates* **2023**, doi:10.1007/s11164-023-05174-5.
4. Zhukova, A.I.; Chuklina, S.G.; Maslenkova, S.A. Study of Cu Modified Zr and Al Mixed Oxides in Ethanol Conversion: The Structure-Catalytic Activity Relationship. *Catal Today* **2021**, *379*, 159–165, doi:10.1016/j.cattod.2021.02.015.
5. Angelici, C.; Weckhuysen, B.M.; Bruijninx, P.C.A. Chemocatalytic Conversion of Ethanol into Butadiene and Other Bulk Chemicals. *ChemSusChem* **2013**, *6*, 1595–1614.
6. Anekwe, I.M.S.; Isa, Y.M.; Oboirien, B. Bioethanol as a Potential Eco-Friendlier Feedstock for Catalytic Production of Fuels and Petrochemicals. *Journal of Chemical Technology and Biotechnology* **2023**, *98*, 2077–2094.
7. Chaichana, E.; Boonsinvarothai, N.; Chitpong, N.; Jongsomjit, B. Catalytic Dehydration of Ethanol to Ethylene and Diethyl Ether over Alumina Catalysts Containing Different Phases with Boron Modification. *Journal of Porous Materials* **2019**, *26*, 599–610, doi:10.1007/s10934-018-0663-7.
8. Haribal, V.P.; Chen, Y.; Neal, L.; Li, F. Intensification of Ethylene Production from Naphtha via a Redox Oxy-Cracking Scheme: Process Simulations and Analysis. *Engineering* **2018**, *4*, 714–721.
9. Ngcobo, M.; Makgwane, P.R.; Mathe, M.K. A Minireview on Solid Acid Catalysts for Dehydration of Bioethanol to Renewable Ethylene: An Update on Catalysts Development Progress. *Applied Catalysis O: Open* **2024**, *193*, 206976, doi:10.1016/j.apcato.2024.206976.
10. Nakagawa, Y.; Yabushita, M.; Tomishige, K. A Perspective on Catalytic Production of Olefinic Compounds from Biomass. *RSC Sustainability* **2023**, *1*, 814–837.
11. Kostestky, P.; Yu, J.; Gorte, R.J.; Mpourmpakis, G. Structure-Activity Relationships on Metal-Oxides: Alcohol Dehydration. *Catal Sci Technol* **2014**, *4*, 3861–3869, doi:10.1039/c4cy00632a.
12. Lv, J.; Wang, D.; Peng, L.; Guo, X.; Ding, W.; Yang, W. Ethanol Dehydration to Ethylene over High-Energy Facets Exposed Gamma Alumina. *Catalysts* **2023**, *13*, doi:10.3390/catal13060994.

13. Ward, D.J.; Saccomando, D.J.; Vilela, F.; Walker, G.; Mansell, S.M. Flow Chemistry Enhances Catalytic Alcohol-to-Alkene Dehydration. *Catal Sci Technol* **2024**, doi:10.1039/d4cy00913d.
14. Manabe, K.; Iimura, S.; Sun, X.M.; Kobayashi, S. Dehydration Reactions in Water. Brønsted Acid-Surfactant-Combined Catalyst for Ester, Ether, Thioether, and Dithioacetal Formation in Water. *J Am Chem Soc* **2002**, *124*, 11971–11978, doi:10.1021/ja026241j.
15. Alharbi, W.; Brown, E.; Kozhevnikova, E.F.; Kozhevnikov, I. V. Dehydration of Ethanol over Heteropoly Acid Catalysts in the Gas Phase. *J Catal* **2014**, *319*, 174–181, doi:10.1016/j.jcat.2014.09.003.
16. Ohayon Dahan, H.; Landau, M. V.; Herskowitz, M. Effect of Surface Acidity-Basicity Balance in Modified Zn<sub>x</sub>Zr<sub>y</sub>O<sub>z</sub> Catalyst on Its Performance in the Conversion of Hydrous Ethanol to Hydrocarbons. *Journal of Industrial and Engineering Chemistry* **2021**, *95*, 156–169, doi:10.1016/j.jiec.2020.12.014.
17. Ouayloul, L.; El Doukkali, M.; Jiao, M.; Dumeignil, F.; Agirrezabal-Telleria, I. New Mechanistic Insights into the Role of Water in the Dehydration of Ethanol into Ethylene over ZSM-5 Catalysts at Low Temperature. *Green Chemistry* **2023**, *25*, 3644–3659, doi:10.1039/d2gc04437d.
18. Wu, C.Y.; Wu, H.S. Ethylene Formation from Ethanol Dehydration Using ZSM-5 Catalyst. *ACS Omega* **2017**, *2*, 4287–4296, doi:10.1021/acsomega.7b00680.
19. Pylinina, A.I.; Akhmedova, L.S.; Knyazeva, E.I.; Fionov, Y.A.; Sokolova, E.A. Acid Properties of Cesium-Nickel-Zirconium Complex Phosphates: Effect on Isobutanol Dehydration. *Petroleum Chemistry* **2020**, *60*, 592–596, doi:10.1134/S0965544120050084.
20. Mayorov, P.; Asabina, E.; Zhukova, A.; Osaulenko, D.; Pet'kov, V.; Lavrenov, D.; Kovalskii, A.; Fionov, A. Catalytic Properties of the Framework-Structured Zirconium-Containing Phosphates in Ethanol Conversion. *Research on Chemical Intermediates* **2021**, *47*, 3645–3659, doi:10.1007/s11164-021-04488-6.
21. Zhukova, A.I.; Asabina, E.A.; Kharlanov, A.N.; Osaulenko, D.A.; Chuklina, S.G.; Zhukov, D.Y.; Pet'kov, V.I.; Deyneko, D. V. Novel Complex Titanium NASICON-Type Phosphates as Acidic Catalysts for Ethanol Dehydration. *Catalysts* **2023**, *13*, doi:10.3390/catal13010185.
22. Povarova, E.I.; Pylinina, A.I.; Mikhalev, I.I. Catalytic Dehydrogenation of Propanol-2 on Na-Zr Phosphates Containing Cu, Co, and Ni. *Russian Journal of Physical Chemistry A* **2012**, *86*, 935–941, doi:10.1134/S0036024412060210.
23. Pavel Mayorov; Elena Asabina; Anna Zhukova; Diana Osaulenko; Vladimir Pet'kov; Dmitry Lavrenov; Andrey Kovalskii; Alexander Fionov Catalytic Properties of the Framework-structured Zirconium-containing Phosphates in Ethanol Conversion. *Research on Chemical Intermediates* **2021**, *47*, 3645–3659.
24. Ermilova, M.M.; Sukhanov, M. V.; Borisov, R.S.; Orekhova, N. V.; Pet'Kov, V.I.; Novikova, S.A.; Il'in, A.B.; Yaroslavl'tsev, A.B. Synthesis of the New Framework Phosphates and Their Catalytic Activity in Ethanol Conversion into Hydrocarbons. *Catal Today* **2012**, *193*, 37–41, doi:10.1016/j.cattod.2012.02.029.
25. Novikova, S.A.; Il'in, A.B.; Zhilyaeva, N.A.; Yaroslavl'tsev, A.B. Catalytic Activity of Li<sub>1</sub> + XHf<sub>2</sub>-XIn<sub>x</sub>(PO<sub>4</sub>)<sub>3</sub>-Based NASICON-Type Materials for Ethanol Conversion Reactions. *Inorganic Materials* **2018**, *54*, 676–682, doi:10.1134/S0020168518070117.
26. Ziyad, M.; Rouimi, M.; Portefaix, J. Activity in Hydrotreatment Processes of Ni-Mo Loaded Zirconium Phosphate Zr<sub>3</sub>(PO<sub>4</sub>)<sub>4</sub>. **1999**, 183.
27. Mitran, G.; Mieritz, D.G.; Seo, D.K. Highly Selective Solid Acid Catalyst H<sub>1</sub>-XTi<sub>2</sub>(PO<sub>4</sub>)<sub>3-x</sub>(SO<sub>4</sub>)<sub>x</sub> for Non-Oxidative Dehydrogenation of Methanol and Ethanol. *Catalysts* **2017**, *7*, 1–13, doi:10.3390/catal7030095.
28. Acosta-Silva, Y. de J.; Lugo-Arredondo, M.I.; Gallardo-Hernández, S.; García-Trejo, J.F.; Matsumoto, Y.; Rivas, S.; Feregrino-Pérez, A.A.; Godínez, L.A.; Méndez-López, A. Comparison of Photocatalytic Activity: Impact of Hydrophilic Properties on TiO<sub>2</sub> and ZrO<sub>2</sub> Thin Films. *Inorganics (Basel)* **2024**, *12*, doi:10.3390/inorganics12120320.
29. Ftouni, J.; Muñoz-Murillo, A.; Goryachev, A.; Hofmann, J.P.; Hensen, E.J.M.; Lu, L.; Kiely, C.J.; Bruijninx, P.C.A.; Weckhuysen, B.M. ZrO<sub>2</sub> Is Preferred over TiO<sub>2</sub> as Support for the Ru-Catalyzed Hydrogenation of Levulinic Acid to  $\gamma$ -Valerolactone. *ACS Catal* **2016**, *6*, 5462–5472, doi:10.1021/acscatal.6b00730.
30. Phung, T.K.; Hernández, L.P.; Busca, G. Conversion of Ethanol over Transition Metal Oxide Catalysts: Effect of Tungsta Addition on Catalytic Behaviour of Titania and Zirconia. *Appl Catal A Gen* **2015**, *489*, 180–187, doi:10.1016/j.apcata.2014.10.025.

31. Danilova, I.G.; Dik, P.P.; Sorokina, T.P.; Gabrienko, A.A.; Kazakov, M.O.; Paukshtis, E.A.; Doronin, V.P.; Klimov, O. V.; Noskov, A.S. Effect of Rare Earths on Acidity of High-Silica Ultrastable REY Zeolites and Catalytic Performance of NiMo/REY+Al<sub>2</sub>O<sub>3</sub> Catalysts in Vacuum Gas Oil Hydrocracking. *Microporous and Mesoporous Materials* **2022**, *329*, doi:10.1016/j.micromeso.2021.111547.
32. De La Puente, G.; Falabella Souza-Aguiar, E.; María, F.; Zotin, Z.; Lúcia, V.; Camorim, D.; Sedran, U. *Influence of Different Rare Earth Ions on Hydrogen Transfer over Y Zeolite*; 2000; Vol. 197.
33. Li, M.; Zhang, J.; Purdy, S.C.; Lin, F.; Unocic, K.A.; Cordon, M.; Wu, Z.; Wang, H.; Hall, J.; Kropf, A.J.; et al. Tailoring Olefin Distribution via Tuning Rare Earth Metals in Bifunctional Cu-RE/Beta-Zeolite Catalysts for Ethanol Upgrading. *Appl Catal B* **2024**, *344*, doi:10.1016/j.apcatb.2023.123648.
34. Yang, Z.; Li, X.; Zhang, R.; Liu, R. Rare Earth Cation-Modified X Zeolites for Isobutane Alkylation: The Influence of Ionic Radius. *Fuel* **2024**, *363*, doi:10.1016/j.fuel.2024.130938.
35. Chiang, H.; Bhan, A. Catalytic Consequences of Hydroxyl Group Location on the Rate and Mechanism of Parallel Dehydration Reactions of Ethanol over Acidic Zeolites. *J Catal* **2010**, *271*, 251–261, doi:10.1016/j.jcat.2010.01.021.
36. Chuklina, S.; Zhukova, A.; Fionov, Y.; Kadyko, M.; Fionov, A.; Zhukov, D.; Il'icheva, A.; Podzorova, L.; Mikhalevko, I. Selectivity of Ethanol Conversion on Al/Zr/Ce Mixed Oxides: Dehydration and Dehydrogenation Pathways Based on Surface Acidity Properties. *ChemistrySelect* **2022**, *7*, doi:10.1002/slct.202203031.
37. Bykov, D.M.; Gobechiya, E.R.; Kabalov, Y.K.; Orlova, A.I.; Tomilin, S. V. Crystal Structures of Lanthanide and Zirconium Phosphates with General Formula Ln<sub>0.33</sub>Zr<sub>2</sub>(PO<sub>4</sub>)<sub>3</sub>, Where Ln=Ce, Eu, Yb. *J Solid State Chem* **2006**, *179*, 3101–3106, doi:10.1016/j.jssc.2006.06.002.
38. Elena A. Asabina; Anna I. Zhukova; Vladislav A. Sedov; Vladimir I. Pet'kov; Diana A. Osaulenko; Ekaterina B. Markova; Diana G. Fukina; Vitalii A. Koshkin Catalytic Characteristics of NASICON-Type Phosphates with Rare Earth Elements in Ethanol Conversion. *Solid State Sci* **2025**.
39. Asabina, E.; Sedov, V.; Pet'kov, V.; Deyneko, D.; Kovalsky, A. Synthesis, Structure and Luminescence Properties of the Europium-Containing NASICON Type Phosphates. *J Solgel Sci Technol* **2023**, *105*, 547–554, doi:10.1007/s10971-022-06028-z.
40. Lightfoot P, W.D.A., J.J.D., S.S. Low Thermal Expansion Materials: A Comparison of the Structural Behaviour of La<sub>0.33</sub>Ti<sub>2</sub>(PO<sub>4</sub>)<sub>3</sub>, Sr<sub>0.5</sub>Ti<sub>2</sub>(PO<sub>4</sub>)<sub>3</sub> and NaTi<sub>2</sub>(PO<sub>4</sub>)<sub>3</sub>. *Int. J. Inorg. Mater* **1999**, *53–60*, doi:https://doi:10.1016/s1463-0176(99)00008-3.
41. Bykov, D.M.; Gobechiya, E.R.; Kabalov, Y.K.; Orlova, A.I.; Tomilin, S. V. Crystal Structures of Lanthanide and Zirconium Phosphates with General Formula Ln<sub>0.33</sub>Zr<sub>2</sub>(PO<sub>4</sub>)<sub>3</sub>, Where Ln=Ce, Eu, Yb. *J Solid State Chem* **2006**, *179*, 3101–3106, doi:10.1016/j.jssc.2006.06.002.
42. Bykov, D.M.; Konings, R.J.M.; Apostolidis, C.; Hen, A.; Colineau, E.; Wiss, T.; Raison, P. Synthesis and Investigation of Neptunium Zirconium Phosphate, a Member of the NZP Family: Crystal Structure, Thermal Behaviour and Mössbauer Spectroscopy Studies. *Dalton Transactions* **2017**, *46*, 11626–11635, doi:10.1039/c7dt02110k.
43. Kurazhkovskaya V. S.; Bykov D. M.; Orlova A. I. Infrared Spectroscopy and Structure of Trigonal Zirconium Orthophosphates with Lanthanides and Actinides. *Journal of Structural Chemistry* **2004**, *45*, 966–973.
44. Davydov Anatoli *Molecular Spectroscopy of Oxide Catalyst Surfaces*; Sheppard N. T., Ed.; Wiley.; Wiley, 2003; ISBN 0-471-9873-X.
45. Pekounov, Y.; Chakarova, K.; Hadjiivanov, K. Surface Acidity of Calcium Phosphate and Calcium Hydroxyapatite: FTIR Spectroscopic Study of Low-Temperature CO Adsorption. *Materials Science and Engineering C* **2009**, *29*, 1178–1181, doi:10.1016/j.msec.2008.10.011.
46. Köck, E.M.; Kogler, M.; Bielz, T.; Klötzer, B.; Penner, S. In Situ FT-IR Spectroscopic Study of CO<sub>2</sub> and CO Adsorption on Y<sub>2</sub>O<sub>3</sub>, ZrO<sub>2</sub>, and Yttria-Stabilized ZrO<sub>2</sub>. *Journal of Physical Chemistry C* **2013**, *117*, 17666–17673, doi:10.1021/jp405625x.
47. Paukshtis, E.A.; Yurchenko, E.N. *Study of the Acid-Base Properties of Heterogeneous Catalysts by Infrared Spectroscopy*; 1983; Vol. 52;.

48. Tsyganenko, A.A.; Filimonov, V.N. *INFRARED SPECTRA OF SURFACE HYDROXYL GROUPS AND CRYSTALLINE STRUCTURE OF OXIDES*;
49. Phillips, C.B.; Datta, R. *Production of Ethylene from Hydrous Ethanol on H-ZSM-5 under Mild Conditions*; 1997;
50. Phung, T.K.; Busca, G. Diethyl Ether Cracking and Ethanol Dehydration: Acid Catalysis and Reaction Paths. *Chemical Engineering Journal* **2015**, *272*, 92–101, doi:10.1016/j.cej.2015.03.008.
51. Asabina, E.A.; Zhukova, A.I.; Sedov, V.A.; Pet'kov, V.I.; Osaulenko, D.A.; Markova, E.B.; Fukina, D.G.; Koshkin, V.A. Catalytic Characteristics of NASICON-Type Phosphates with Rare Earth Elements in Ethanol Conversion. *Solid State Sci* **2025**, 107865, doi:10.1016/j.solidstatesciences.2025.107865.
52. Inaba, M.; Murata, K.; Takahara, I.; Inoue, K.I. Production of C<sub>3</sub>+ Olefins and Propylene from Ethanol by Zr-Modified H-ZSM-5 Zeolite Catalysts. *Advances in Materials Science and Engineering* **2012**, *2012*, doi:10.1155/2012/293485.
53. Chen, Y.; Wu, Y.; Tao, L.; Dai, B.; Yang, M.; Chen, Z.; Zhu, X. Dehydration Reaction of Bio-Ethanol to Ethylene over Modified SAPO Catalysts. *Journal of Industrial and Engineering Chemistry* **2010**, *16*, 717–722, doi:10.1016/j.jiec.2010.07.013.
54. Phung, T.K.; Hernández, L.P.; Busca, G. Conversion of Ethanol over Transition Metal Oxide Catalysts: Effect of Tungsta Addition on Catalytic Behaviour of Titania and Zirconia. *Appl Catal A Gen* **2015**, *489*, 180–187, doi:10.1016/j.apcata.2014.10.025.
55. Domoroshchina, E.; Kravchenko, G.; Kuz'micheva, G.; Markova, E.; Zhukova, A.; Pirutko, L.; Khramov, E.; Dorokhov, A.; Koroleva, A. The Role of the Compositions of HZSM-5 Zeolites Modified with Nanosized Anatase in Propane and Ethanol Conversion. *Catal Today* **2022**, *397–399*, 511–525, doi:10.1016/j.cattod.2021.06.021.
56. Garbarino, G.; Prasath Parameswari Vijayakumar, R.; Riani, P.; Finocchio, E.; Busca, G. Ethanol and Diethyl Ether Catalytic Conversion over Commercial Alumina and Lanthanum-Doped Alumina: Reaction Paths, Catalyst Structure and Coking. *Appl Catal B* **2018**, *236*, 490–500, doi:10.1016/j.apcatb.2018.05.039.
57. Phung, T.K.; Busca, G. Diethyl Ether Cracking and Ethanol Dehydration: Acid Catalysis and Reaction Paths. *Chemical Engineering Journal* **2015**, *272*, 92–101, doi:10.1016/j.cej.2015.03.008.
58. Phung, T.K.; Lagazzo, A.; Rivero Crespo, M.Á.; Sánchez Escribano, V.; Busca, G. A Study of Commercial Transition Aluminas and of Their Catalytic Activity in the Dehydration of Ethanol. *J Catal* **2014**, *311*, 102–113, doi:10.1016/j.jcat.2013.11.010.
59. Asabina, E.A.; Pet'kov, V.I.; Stenina, I.A.; Yaroslavtsev, A.B. Synthesis and Ionic Conductivity of Na<sub>1+2x</sub>M<sub>x</sub>Zr<sub>2-x</sub>(PO<sub>4</sub>)<sub>3</sub> (M – Mg, Mn) NASICON-Type Ceramic Materials. *Solid State Sci* **2025**, *160*, doi:10.1016/j.solidstatesciences.2024.107786.
60. Badmaev, S.D.; Smorygina, A.S.; Paukshtis, E.A.; Belyaev, V.D.; Sobyenin, V.A.; Parmon, V.N. Gas-Phase Carbonylation of Dimethoxymethane to Methyl Methoxyacetate on Solid Acids: The Effect of Acidity on the Catalytic Activity. *Kinetics and Catalysis* **2018**, *59*, 99–103, doi:10.1134/S0023158418010020.

**Disclaimer/Publisher's Note:** The statements, opinions and data contained in all publications are solely those of the individual author(s) and contributor(s) and not of MDPI and/or the editor(s). MDPI and/or the editor(s) disclaim responsibility for any injury to people or property resulting from any ideas, methods, instructions or products referred to in the content.